Available online at www.sciencedirect.com
SCIENCE DIRECT®
ELSEVIER
Earth and Planetary Science Letters 216 (2003) 201–208
EPSL
www.elsevier.com/locate/epsl

Production rates of cosmogenic nuclides in boulders

Jozef Masarik [a], Rainer Wieler [b,*]

[a] *Department of Nuclear Physics, Komensky University, Bratislava, Slovak Republic*
[b] *ETH Zürich, Isotope Geology and Mineral Resources, NO C61, CH-8092 Zürich, Switzerland*

Received 17 March 2003; received in revised form 20 August 2003; accepted 29 August 2003

Abstract

We study how the production rates of cosmogenic nuclides in solid targets at the Earth's surface depend on the shape and size of a sampled rock and the position of a sample. We use a physical model simulating the interaction of galactic cosmic ray particles with matter. Production rates at boulder surfaces may be up to 10–12% lower than values at the surface of an infinite flat target of the same chemical composition, even when the former sample sees cosmic rays from the full 2π solid angle. This is because cosmic ray neutrons are more easily lost back to the atmosphere from within a non-flat sample than from a flat surface. Therefore, the shape and size of a boulder need to be considered when taking samples, and production rates may have to be corrected accordingly.

Keywords: cosmogenic nuclides; exposure dating; production rates

1. Introduction

Nuclides produced by cosmic rays in solid targets at the Earth's surface are a major tool in quantitative geomorphology [1,2]. Apart from the chemical composition of the target, the production rates of these cosmogenic nuclides mainly depend on the 'shielding' of a sample, a somewhat loose term subsuming the attenuation or blocking of the cosmic ray flux by the geomagnetic field, the atmosphere, overlying material and obstacles on the horizon or nearby. The effects of the geomagnetic field and the atmosphere have been discussed in [3–7] and the variations of production rates with depth below the surface of a rock are also well studied (e.g. [8]). Corrections for objects on the horizon or for samples taken from a non-horizontal but flat surface are described in [1,9]. The temporal variation of the paleomagnetic field strength can also be taken into account [7,10,11].

A further factor influencing the flux of cosmic ray neutrons and hence production rates is the shape of the irradiated rock. For example, the total neutron flux on the top of a hemispheric boulder lying on a large otherwise flat surface will be lower than the flux at zero depth somewhere nearby on the flat surface itself, even though both samples see the same flux of incoming neutrons from the entire 2π solid angle. This is because the sample on the flat surface will see more cosmic ray neutrons scattered from sur-

* Corresponding author. Tel.: +41-1-632-3732; Fax: +41-1-632-1179.
E-mail addresses: masarik@fmph.unib.sk (J. Masarik), wieler@erdw.ethz.ch (R. Wieler).

0012-821X/03/$ – see front matter © 2003 Elsevier B.V. All rights reserved.
doi:10.1016/S0012-821X(03)00476-X

rounding rock than the sample at the top of the boulder, i.e. neutrons lost to the atmosphere from the boulder are less well 'compensated' by neutrons from the surrounding rock than is the case in a flat target.

This 'shape effect' is rarely taken into account. Masarik et al. [12] calculated that for a hemispheric boulder of 1 m radius the production rate at the surface averaged over the entire hemisphere is lower by ~11% than the production rate at the surface of a flat target. Such variations are of the same order as or larger than other production rate corrections sometimes applied, e.g. for snow or vegetation cover or intensity changes of the paleomagnetic field. In this work, we therefore extend the calculations of Masarik et al. [12] by studying a broader range of boulder sizes and besides hemispheres other shapes such as cubes and spires. Note that recently a related problem has been treated by Dunne and Elmore [13], namely the variability of the cosmogenic neutron flux in a vertical cliff face near the bottom of the cliff.

2. Model calculations

The model of the simulation of interactions of primary and secondary cosmic ray particles with matter is based on the codes GEANT [14] and MCNP [15]. The modifications of the codes necessary for cosmogenic nuclide production rate calculations are described in detail in [16] and references therein, as are extensive tests proving the reliability of these calculations. Here we only note the main features relevant for the present study.

In our simulations, only primary protons with energies between 10 MeV and 100 GeV were considered. The characteristic feature of the particle interactions at these energies is the production of the cascade of secondary particles. For these calculations the Earth's atmosphere was modeled as a spherical shell with an inner radius of 6378 km and a thickness of 100 km, with an elemental composition (in weight %) of: 75.5% N, 23.2% O, and 1.3% Ar. The total thickness of the atmosphere was taken as 1033 g cm^{-2}, hence all calculations were performed for targets at sea level. The elemental composition of the rocks was assumed to be that of average terrestrial crust (in wt%: 0.2% H, 47.3% O, 2.5% Na, 4.0% Mg, 6.0% Al, 29.0% Si, 5.0% Ca and 6.0% Fe) but the calculated fluxes depend very little on the assumed composition or the addition of other elements such as K, unless very high H contents would be adopted. We adopt a rock density of 2 g cm^{-3}. Control calculations showed, however, that varying the density hardly influences the results. For example, for densities of 2 and 3 g cm^{-3}, respectively, the ratio of correction factors given below for a sphere of 2 m radius is always within 1% of unity. This behavior is somewhat different from that of neutrons in the epithermal and thermal energy range, where previous experience has shown that neutron fluxes and scattering depend more on elemental composition and density than for higher energy neutrons relevant here.

Production rates in an infinite flat target at various depths (used for normalization purposes) were obtained by dividing the target into horizontal layers of a thickness of 5 cm. Proton and neutron fluxes within each layer were calculated first. Production rates of cosmogenic nuclides were then obtained by integrating over energy the product of these fluxes with cross sections for all nuclear reactions producing the nuclide under investigation. The calculations presented below were all done for the nuclide ^{10}Be. However, we expect that within errors imposed by statistics of the calculations, these results are well valid for all cosmogenic nuclides produced mainly by spallation reactions (i.e. for all nuclides of interest except ^{36}Cl), because we are interested in production rate differences imposed by geometry rather than in absolute production rates. This has been verified in the case of ^{26}Al production in the $R = 1$ m hemisphere. The normalized ^{26}Al and ^{10}Be production rates indeed agree with each other well within error limits.

The main purpose of this work is to study production rates in rocks of various shapes (which are all assumed to lie on an infinite flat surface). Proton and neutron fluxes within these rocks were calculated by dividing the rocks into cells basi-

cally with linear dimensions of 5 cm (for the hemispheric boulders also hemispheric shells of 5 cm thickness were considered). An important modification with respect to the calculations for flat targets was that we used the fluxes from a hemispheric source with a radius of 20 m as input for the simulations. This source emitted particles with a flux corresponding in spectral and angular distribution to the respective values at 20 m above ground (the error introduced by adopting the flux at 20 m above ground over the entire hemisphere is negligible, because the flux of neutrons hardly varies within the first 20 m above ground and because the transport of all particles within the hemisphere has been simulated). The rocks in the center of this hemisphere were irradiated with 5 million particles. The chosen radius of 20 m is a compromise between the statistical efficiency of the calculations and the requirement not to miss any particles that might interact with the rock, e.g. all particles that hit the irradiated object after they were scattered or escaped from the surrounding flat surface or were scattered in the atmosphere. While calculational efficiency decreases with increasing radius, more particles are missed if a smaller source radius is adopted. The further procedure for production rate calculations was then identical with that used for a flat geometry.

The statistical errors of the calculated neutron fluxes were on the level of 2–3% (1σ). The systematic uncertainties of our calculated fluxes are estimated to be on the level of 10%, but these essentially cancel out in the final results. Note that all calculations as well as the normalization of the results take into account that neutron fluxes in the first 10–20 g cm^{-2} below the air–rock interface are rather constant [17]. For the cross sections of the relevant nuclear reactions we relied on the values evaluated and tested in earlier calculations [8] and updated with new values from recent experiments [18–20]. The incoming primary galactic cosmic ray particle flux on the top of the atmosphere was taken to be 4.56 cm^{-2} s^{-1}. The secondary particle flux at ground as a function of the azimuth angle Θ is usually described by $\cos^n\Theta$. Our calculated fluxes correspond to a best fit value of n of 2.65.

3. Results and discussion

3.1. Thin columns

Fig. 1 shows the production rates in the top 5 cm of five thin vertical columns of variable length standing on a flat horizontal surface. Each column has a quadratic cross section of 5×5 cm. Production rates are normalized to the mean value in the top 5 cm of the flat surface. This geometry serves well to illustrate the main effect discussed here. The missing mass around the column clearly manifests itself, since the production rates at the top of each column are lower than the value at the top of the flat surface, although the shielding is essentially zero in both cases and although all samples see incoming cosmic rays from the entire 2π solid angle. Whereas the production rate is reduced by a mere 2% at the top of the 0.2 m column, the reduction amounts to some 10% at the top of the 1 m column, an effect that clearly cannot be neglected. Quite remarkably, the production rates at the top of the 1.5 and 2 m columns are only a little lower than the value at the top of the 1 m column.

In summary, Fig. 1 illustrates that for samples which have at least one dimension comparable to the interaction length of the reacting particles, the real geometry has to be considered. The reason is that particles escaping from such samples are not

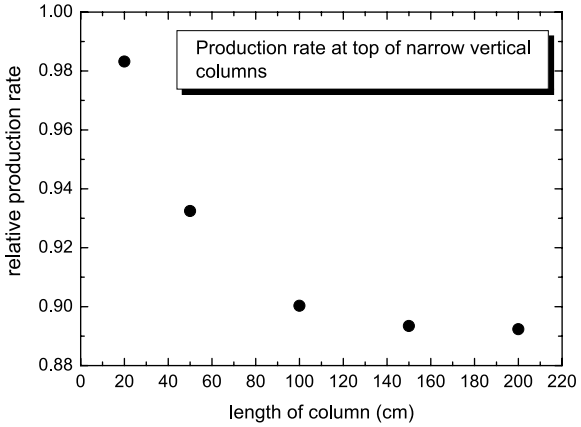

Fig. 1. Mean production rate of cosmogenic nuclides in the top 5 cm of five vertical columns with a cross section of 5×5 cm, normalized to the mean production rate in the top 5 cm layer of a flat infinite surface.

compensated to the same extent by particles scattered from other parts of the target as would be the case in a flat surface. Next we will study boulder shapes of more immediate practical interest.

3.2. Hemispheres

The inset of Fig. 2a shows for hemispherical boulders of various radii the production rate averaged over the entire hemispheric shell at depth d, normalized to the respective production rate at depth d in a flat infinite target. This is an extension of the work of Masarik et al. [12]. The figure shows that neutron flux reductions are largest for boulders of about 1 m size (small differences between the $R=1$ m curve shown here and in [12] are due to improved statistics and because we now consider that the boulder is surrounded by air and not vacuum).

Perhaps of more practical interest than the production rate averaged over a hemispheric shell is the value at any given position. This is shown in the main panel of Fig. 2A and in Fig. 2B. Fig. 2A shows the production rates in the top 5 cm layer of each of four spheres. The abscissa represents the angle formed by the vertical and the radius line passing through the sample. Again, the production rates are normalized to those in the top 5 cm of an infinite flat surface.

Only at the top of a hemisphere (angle 0 in Fig. 2A) is a calculated production rate reduction entirely due to the neutron flux deficit caused by the 'missing mass', whereas at all other positions part of the reduction will be due to shielding of the incoming cosmic ray particles by the boulder itself. Hence, Fig. 2B shows that the missing mass effect which we primarily study here reduces the production rate by some 4.5% at the top of a $R=1$ m boulder and even somewhat less than that at all other sizes. On the other hand, in samples taken from the surface but away from the symmetry axis of the boulder, the combined reduction caused by self-shielding and missing mass amounts to up to $\sim$13% for surface samples taken close to the bottom of a $R=1$ m hemispheric boulder. Since samples usually will be taken from the top of a boulder, it is perhaps gratifying that the required corrections at this position do not exceed about 4%. Note, however, that corrections for, e.g., snow cover or self-shielding due to finite sample thickness are often even considerably smaller and yet are routinely done. That the correction shows a maximum at one particular radius is expected, since the irradiation geometry of both very large and very small boulders will effectively be similar to that of a flat surface.

The main panel of Fig. 2B shows the production rate at depth d along straight lines through the center of a $R=1$ m hemisphere at various angles to the vertical, and the inset of the figure shows the same for a $R=0.5$ m hemisphere. All production rates are normalized to the value at the same depth d in a flat target. The fact that not all lines pass exactly through the same value at the center reflects the statistical uncertainties of the calculations. Normalized production rates at the center are only slightly below unity in the smaller boulder, and only slightly above unity in the larger one. This may seem to be rather surprising, since at the center of a hemisphere the shielding integrated over the entire 2π solid angle is substantially lower than at depth R in a flat target. Apparently this lower shielding just about compensates the 'missing mass' effect. This is presumably due to several factors: (i) the flux of galactic cosmic ray particles incident at a low angle relative to the horizontal is minor, which means that the larger shielding in the flat target is less important than it may seem, (ii) near the center of the hemisphere, the escape of particles is probably not so different from that at depth R in the flat target, and (iii) the contributions from particles scattered from the surroundings is minor at larger depths.

3.3. Cubes

Fig. 3 shows the results for cubic boulders with sizes varying between 0.5 and 3 m. Again, the cubes lie on an otherwise flat surface. Normalized production rates are shown for the top surface layer of 5 cm thickness, along two straight lines. One of them (represented by solid lines in Fig. 3) connects the center of the top face with the center of a top edge of the cube, the other one (dashed

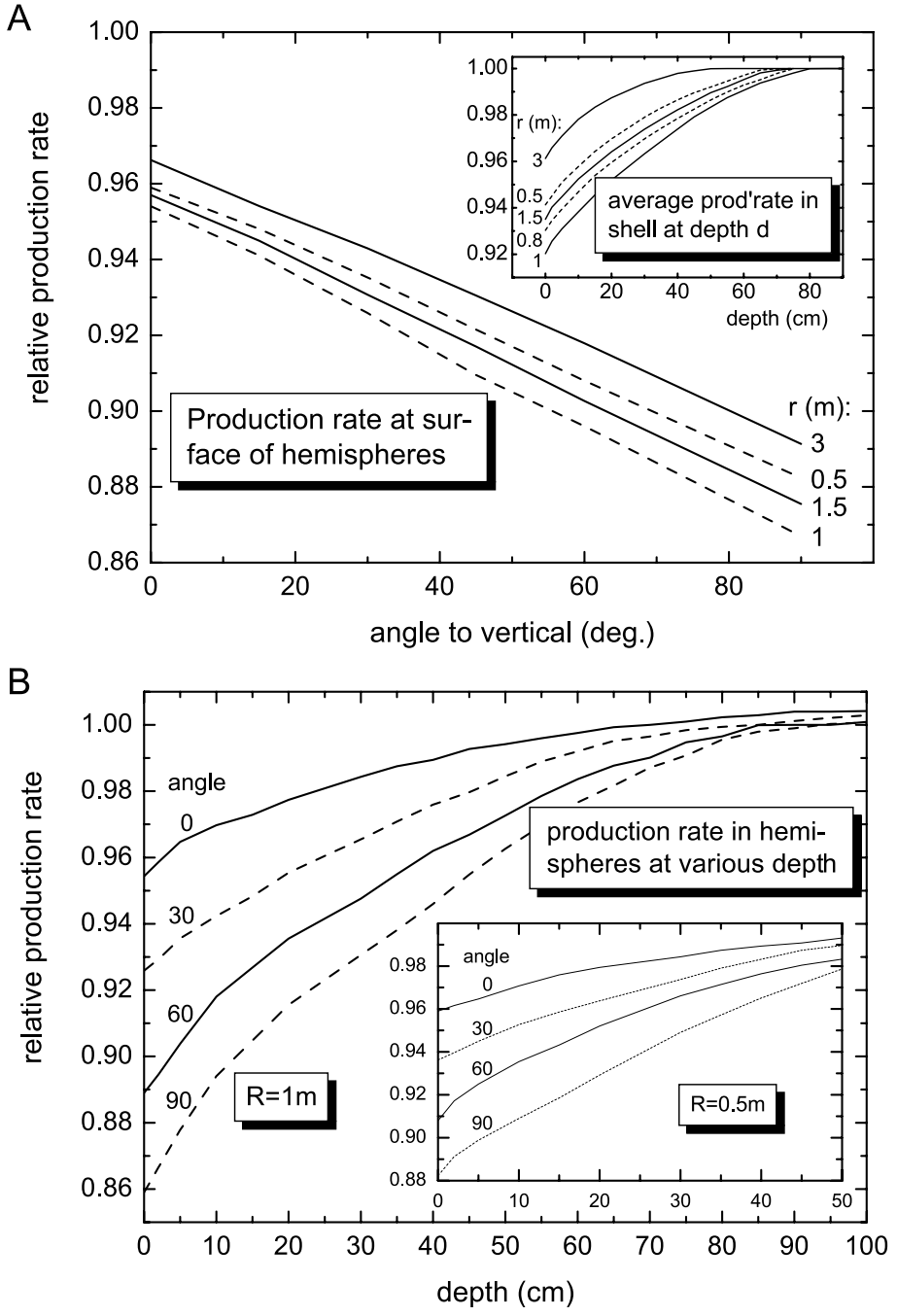

Fig. 2. (A) Main panel: Production rate at a given position in the top layer (5 cm) of four hemispherical boulders with radii between 0.5 and 3 m. The abscissa represents the angle formed by the vertical and the radius line passing through the sample. Production rates are normalized to those in top 5 cm of an infinite flat surface. Inset: Production rate averaged over the entire hemispheric shell at depth d, normalized to the respective value at depth d in a flat infinite target. (B) Main panel: Production rate at depth d along straight lines through the center of a $R=1$ m hemisphere at various angles to the vertical. Inset: the same for $R=0.5$ m. All production rates are normalized to the value at the same depth d in a flat target.

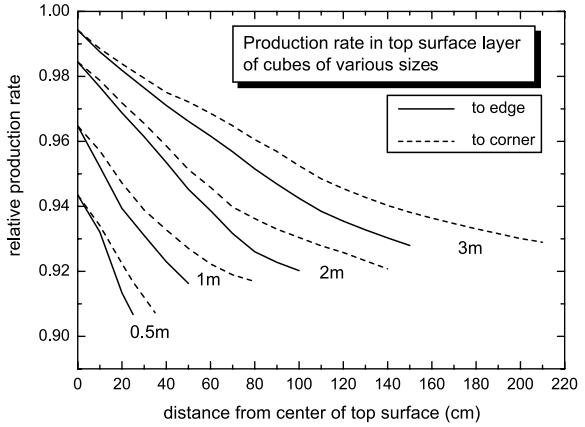

Fig. 3. Normalized production rates for four different cubic boulders. Shown are values for the top surface layer (5 cm) along two straight lines, both extending from the center of the top face, one towards the center of an edge, the other towards a corner. Production rates are normalized to the average value in the top 5 cm of an infinite flat target.

lines in Fig. 3) is a diagonal on the top face. The abscissa represents the distance from the center of the top face. Production rates are normalized to the average value in a layer of 5 cm thickness at the surface of an infinite flat target.

In contrast to the hemispheric geometry, Fig. 3 shows exclusively the influence of the 'missing mass', because all samples are unshielded (apart from the shielding due to the finite layer thickness, which is identical to that used for the normalization). As expected, production rates decrease from the center of the cube's top surface towards the edges and the corners. Whereas corrections are nearly negligible for samples from the center of the top face of a 3 m boulder, corrections on the order of 5–10% are necessary for all samples from a 50 cm boulder but also for samples from near the edges or corners of larger boulders. Corrections for samples from a corner of a given cube differ only very slightly from those for a sample from the center of an edge of the same cube.

3.4. Pyramids

The last geometry we consider is pyramids with a square base and with a vertical symmetry axis passing through the center of the base. Fig. 4 shows the results for three such pyramids. Two of them have the same base of 1×1 m but differ in their height (1 and 2 m, respectively), whereas the third pyramid has a base length of 2 m and is 1 m high. Shown is the relative production rate in the top meter along the vertical passing through the symmetry axis (i.e. the top of the pyramid is at $d = 0$). Normalization is relative to the production rate at depth d in a flat target. The figure shows that production rates for samples from the tip of all three pyramids need a sizeable correction of the order of 10%, whereby the correction only slightly depends on the angle formed by the faces of the pyramid. As expected, the smaller this angle is, the larger the correction becomes.

3.5. Comparison with data

To our knowledge only very few data exist with which to compare the calculations presented here. One such set is provided by Gosse et al. [21], who measured ^{10}Be in samples from the centers of horizontal surfaces on the top of about 10 boulders of variable size deposited on the Inner Titcomb Lakes moraine in the Wind River Mountains, WY, USA. Concentrations of cosmogenic ^{10}Be corrected for snow cover vary by 7–10% for boulder sizes between 0.1 and 2 m. Interestingly, the lowest values are all found for boulders of 1 m

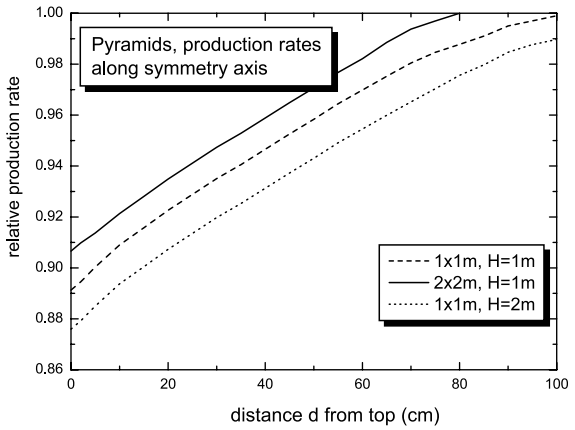

Fig. 4. Normalized production rate in the top meter along the vertical passing through the symmetry axis of three different pyramids. Production rates are normalized to the value at depth d in a flat target.

size, whereas both smaller and larger boulders show higher concentrations. This dataset is certainly too limited to allow for a firm comparison with our model results, but we note that the observed variations are of the same order as the predicted ones and their appears to be a minimum at one particular boulder size. Clearly, however, systematic studies of nuclide concentrations on various positions of suitable boulders will be an important next step.

4. Summary and conclusions

We have shown that the production rates of cosmogenic nuclides depend on the shape and size of a sampled rock not only in the obvious cases where surface samples do not see the full 2π solid angle due to self-shielding by the rest of the rock. In samples from non-flat geometries the cosmic ray neutron flux is usually lower than in a sample residing in a flat target because the number of scattered neutrons lost from the target to the atmosphere is larger in non-flat targets. We show that this effect is largest at the surface of a boulder. Corrections for production rate calculations amount to up to 10–12%, e.g. for samples taken at a top edge of a cubic boulder of 0.5–2 m size or at the top of a $\sim$1–2 m sized pyramid. Such corrections may thus be of the same order or larger than other corrections sometimes made, e.g. for snow or vegetation cover or intensity changes of the paleomagnetic field. Therefore, the shape and size of a boulder have to be considered when taking samples, and, if necessary, production rates need to be corrected accordingly. A further consequence of this work is that, if possible, samples should be taken from some inner part of a flat face of a boulder, although it is often considerably easier to remove material from a corner or an edge.

Erosion has not been considered in the calculations here. For obviously eroded boulders, the production rate uncertainty due to erosion may exceed the one due to boulder shape, even if the erosion rate may be constrained by analyzing more than one nuclide. So, the correction discussed here is primarily of interest for rather young samples or samples from arid zones with very low erosion rates.

Acknowledgements

We thank the Slovak Grant Agency VEGA for partial support of this research and ETH for financial support of J. M.'s stay in Zürich. We also thank EAWAG/ETH for providing computer time. John Gosse and an anonymous reviewer provided helpful reviews. In particular we thank John Gosse for bringing to our attention the dataset from the Wind River Range and for providing us with the respective raw data.*[KF]*

References

[1] J.C. Gosse, F.M. Phillips, Terrestrial in situ cosmogenic nuclides: theory and application, Quat. Sci. Rev. 20 (2001) 1475–1560.
[2] S. Niedermann, Cosmic-ray-produced noble gases in terrestrial rocks: Dating tools for surface processes, Rev. Min. Geochem. 47 (2002) 731–784.
[3] D. Lal, Cosmic ray labeling of erosion surfaces: in situ nuclide production rates and erosion models, Earth Planet. Sci. Lett. 104 (1991) 424–439.
[4] J. Stone, Air pressure and cosmogenic isotope production, J. Geophys. Res. Solid Earth 105 (B10) (2000) 23753–23759.
[5] T.J. Dunai, Scaling factors for production rates of in situ produced cosmogenic nuclides: a critical reevaluation, Earth Planet. Sci. Lett. 176 (2000) 157–169.
[6] D. Desilets, M. Zreda, On scaling cosmogenic nuclide production rates for altitude and latitude using cosmic-ray measurements, Earth Planet. Sci. Lett. 193 (2001) 213–225.
[7] D. Desilets, M. Zreda, Spatial and temporal distribution of secondary cosmic-ray nucleon intensities and applications to in-situ cosmogenic dating, Earth Planet. Sci. Lett. 206 (2003) 21–42.
[8] J. Masarik, R.C. Reedy, Effects of bulk composition on nuclide production processes in meteorites, Geochim. Cosmochim. Acta 58 (1994) 5307–5317.
[9] J. Dunne, D. Elmore, P. Muzikar, Scaling factors for the rates of production of cosmogenic nuclides for geometric shielding and attenuation at depth on sloped surfaces, Geomorphology 27 (1999) 3–11.
[10] T.J. Dunai, Influence of secular variation of the geomagnetic field on production rates of in situ produced cosmogenic nuclides, Earth Planet. Sci. Lett. 193 (2001) 197–212.

[11] J. Masarik, M. Frank, J.M. Schäfer, R. Wieler, Correction of in situ cosmogenic nuclide production rates for geomagnetic field intensity variations during the past 800,000 years, Geochim. Cosmochim. Acta 65 (2001) 2995–3003.

[12] J. Masarik, D. Kollar, S. Vanya, Numerical simulation of in situ production of cosmogenic nuclides: Effects of irradiation geometry, Nucl. Instrum. Methods B 172 (2000) 786–789.

[13] J.A. Dunne, D. Elmore, Monte Carlo simulations of low-energy cosmogenic neutron fluxes near the bottom of cliff faces, Earth Planet. Sci. Lett. 206 (2003) 43–49.

[14] B. Brun et al., GEANT3 User's Guide, Rep. DD/EE/84-1, 1987, 584 pp.

[15] J.F. Briesmeister, MCNP – A General Monte Carlo N-particle Transport Code Version 4A, Los Alamos Natl. Lab. Publ. LA-12625-M, 1993, 693 pp.

[16] J. Masarik, J. Beer, Simulation of particle fluxes and cosmogenic nuclide production in the Earth's atmosphere, J. Geophys. Res. 104 (D10) (1999) 12099–12111.

[17] J. Masarik, R.C. Reedy, Terrestrial cosmogenic-nuclide production systematics calculated from numerical simulations, Earth Planet. Sci. Lett. 136 (1995) 381–395.

[18] R. Bodemann, H.J. Lange, I. Leya, R. Michel, T. Schiekel, R. Rösel, U. Herpers, H.J. Hofmann, B. Dittrich, M. Suter, W. Wölfli, B. Holmqvist, H. Condé, P. Malmborg, Production of residual nuclei by proton-induced reactions on C, N, O, Mg, Al, and Si, Nucl. Instrum. Methods B 82 (1993) 9–31.

[19] R. Michel, M. Gloris, H.-J. Lange, I. Leya, M. Lüpke, U. Herpers, B. Dittrich-Hannen, R. Rösel, T. Schiekel, D. Filges, P. Dragovitsch, M. Suter, H.-J. Hofmann, W. Wölfli, P.W. Kubik, H. Baur, R. Wieler, Nuclide production by proton-induced-reactions on elements ($6 \geq Z \geq 29$) in the energy range from 800 MeV to 2600 MeV, Nucl. Instrum. Methods B 103 (1995) 183–222.

[20] R. Michel, R. Bodemann, H. Busemann, R. Daunke, M. Gloris, H.-J. Lange, B. Klug, A. Krins, I. Leya, M. Lüpke, S. Neumann, H. Reinhardt, M. Schnatz-Büttgen, U. Herpers, T. Schiekel, F. Sudbrok, B. Holmqvist, H. Condé, P. Malmborg, M. Suter, B. Dittrich-Hannen, P.W. Kubik, H.A. Synal, D. Filges, Cross sections for the production of residual nuclides by low- and medium-energy protons from the target elements C, N, O, Mg, Al, Si, Ca, Ti, V, Mn, Fe, Co Ni, Cu, Sr, Y, Zr, Nb, Ba, and Au, Nucl. Instrum. Methods B 129 (1997) 153–193.

[21] J.C. Gosse, E.B. Evenson, J. Klein, B. Lawn, R. Middleton, Precise cosmogenic ^{10}Be measurements in western North America: Support for a global Younger Dryas cooling event, Geology 23 (1995) 877–880.